*Int. J. Electrochem. Sci.*, 15 **(2020)** 7633 – 7645, doi: 10.20964/2020.08.32

International Journal of
ELECTROCHEMICAL
SCIENCE
www.electrochemsci.org

*Short Communication*

# A New Approach in Recycling Waste Foundry Sand for the Preparation of Porous Silicon Powder

*Rongfu Xu*[*]*, Yueya Shi, Changhou Li, Yong Xu*

School of Materials Science and Engineering, Shandong Jianzhu University, Ji'nan 250101, Shandong, China
[*]E-mail: xrf168@163.com

*Received:* 1 April 2020 / *Accepted:* 20 May 2020 / *Published:* 10 July 2020

Disposal of waste foundry sand is still one of the most critical challenges faced by the foundry industry. The recycling and reusing of waste foundry sand not only lead to a saving of naturally abundant sand sources but also enhance the sustainability of environmental protection. A new approach in recycling waste foundry sand is introduced in the paper. Based on this approach, porous silicon powder is scalably fabricated, employing magnesiothermic reduction. In the initial one cycle, the capacities of the charge and discharge are 2210 mAh/g and 1602 mAh/g, respectively. The coulombic efficiency of the as-prepared porous silicon is about 72%. The as-prepared porous silicon is considered as the potential material for the preparation of silicon-based anodes in high energy Li-ion batteries.

**Keywords:** waste foundry sand; porous silicon; magnesiothermic reduction; Li-ion battery

## 1. INTRODUCTION

Foundry is one of the basic forming processes for mechanical parts. According to the Modern Casting Census of world casting production[1], global casting production amounted to ~109.8 million metric tons in 2017. Foundry silica sand is widely used in the production of casting, due to it is readily available, inexpensive, resistance to heat damage and quickly bonded with the binder in mold or core sand making. The production of casting plants generates a waste product, so-called waste foundry sand (WFS). Foundry industries have been successfully recycled and reused the sand many times in production[2-6]. Cast iron foundries create a massive scale of WFS during the casting process, about one ton of waste sands per one ton of castings[7]. Disposal of WFS remains one of the most critical challenges faced by the foundry industry. The recycling and reusing of waste foundry sand not only lead to a saving of naturally abundant sand sources but also enhance the sustainability of environmental protection[8, 9]. The utilization of WFS has become a popular research topic in recent years[10-12].

Although WFS contains a variety of components such as fines, green sand, resin-bonded core sand, and metallic or nonmetallic impurities, the current study pays excellent attention to the recycling of the available foundry silica sand. As is well known, the $SiO_2$ in foundry sand plays an essential role in resistance to heat damage by molten metal pouring into the moulds at a higher temperature (>1300°C). As for the foundry silica sand, the content of $SiO_2$ is usually over 85% to meet the requirement of casting production. It is a very concerning issue on how to utilize the abundant silicon (Si) resources in foundry sand, especially WFS. Accordingly, it is an excellent opportunity for future research to pursue more useful applications. To recycle WFS upon more valuable applications, WFS processing porous structures materials is achieved by reducing the $SiO_2$ to porous Si in the paper.

With the development of society, the growing appetite for more advanced hybrid electric vehicles and portable electronic devices has accelerated the demands of the high-capacity energy storage batteries. As an essential component of the battery, Si-based anodes have recently attracted full attention due to its high theoretical capacity of about 4200mAh/g[13-16], which is much higher than that of conventional carbon-based anodes(370mAh/g)[17]. However, there is a cycling capacity fading significantly for Si-based anodes in applications. This is mainly ascribed to its low electronic conductivity and more considerable volume expansion, up to about 300% during the charging-discharging process[18]. Besides, the formation of unstable solid electrolyte interphase (SEI) layer towards cycling causes poor cycling performance[19-22]. Accordingly, to alleviate the problems of Si-based anodes described above, scholars from home and abroad have been carried out a large number of targeted research, such as Si in the form of nanostructures, hollow nanoparticles, porous structures[23-25].

The porous structure of materials is a more effective way for battery performance. Besides, the porous materials become a research focus to accommodate the volume expansion during the lithiation process. And porous structures are possibly commercial for the silicon-based anodes. The magnesiothermic reduction is a simple and inexpensive way to fabricate porous Si through converting somethings (such as rice husks, beach sands) or solid silica at about 650°C. In the last few years, the magnesiothermic reduction method has been widely applied to fabricate porous silicon. Some researches, such as Favors used beach sands as raw materials to fabricate porous nano-silicon by magnesiothermic reduction and referred it as electrodes[26]. Shen successfully fabricated the three-dimensional porous silicon by magnesiothermic reducing diatomaceous earth[27]. Liu used rice husks as raw materials to fabricate pure silicon nanoparticles by the magnesiothermic reduction method[28]. Through the magnesiothermic reduction reaction, various silica sources can be used to fabricate Si at a relatively low temperature. Although the desired structure of Si-based anodes has been demonstrated as superior performance for LIB anodes[29-31], the remaining problems are related to large-scale fabricate Si-based anodes at a low cost can be produced in industrial mass production. Several approaches that have been described in the literature to obtain the desired porous Si materials are metal-assisted chemical etching[32], magnesiothermic reduction[33-37], and dealloying method[38-40]. Even though the approaches mentioned above, can be able to fabricate porous silicon with excellent electrochemical properties for electrode, they are not meeting the volume-produced requirement of Si-based anodes due to limited resources raw materials.

In the current study, magnesiothermic reduction, which generates silicon by reducing silica with metallic magnesium, has been aroused broad public concern due to it can adopt low-cost WFS as Si

sources to fabricate porous Si materials. In the paper, the waste foundry sand containing resin-bonded core sand is selected as the research object. A new approach in recycling waste foundry sand for the preparation of porous Si powders is investigated. The factors, such as heating temperature and heating time, the effect on the structure and morphology of the as-prepared porous Si, are investigated, respectively.

## 2. MATERIALS AND METHODS

### *2.1 Preparation of porous Si powders*

The original WFS containing resin-bonded core sand, as raw materials, utilized in the current study were obtained as a by-product of casting production. Magnesium powders (Mg, 200-mesh) and pure silica sand ($SiO_2$ >99.0%) powders were purchased from Aladdin.

To remove organic components for resin-bonded core sand in the original WFS, a thermal treatment was carried on at 700°C for about 2h to obtain calcined WFS. The calcined WFS were leached with water to remove clay or bentonite. The composition of the processed WFS is mainly $SiO_2$ (wt.% ≈ 92%). The desired WFS powder was fabricated by zirconia balls (10mm, 8mm, 6mm, and 5mm) into a zirconia vial (150 mL) with a ball-to-WFS mass ratio of 5:1. The high-energy ball-milling was performed on a rotating speed of 300rpm at room temperature for 6 h to obtain minimal particle size. The ball-milled product was sieved with a 300-mesh iron sieve in this study. In other words, the average particle size of the ball-milled foundry sand was about 300 mesh. After these four steps, the ball-milled powders for the magnesiothermic reduction was produced.

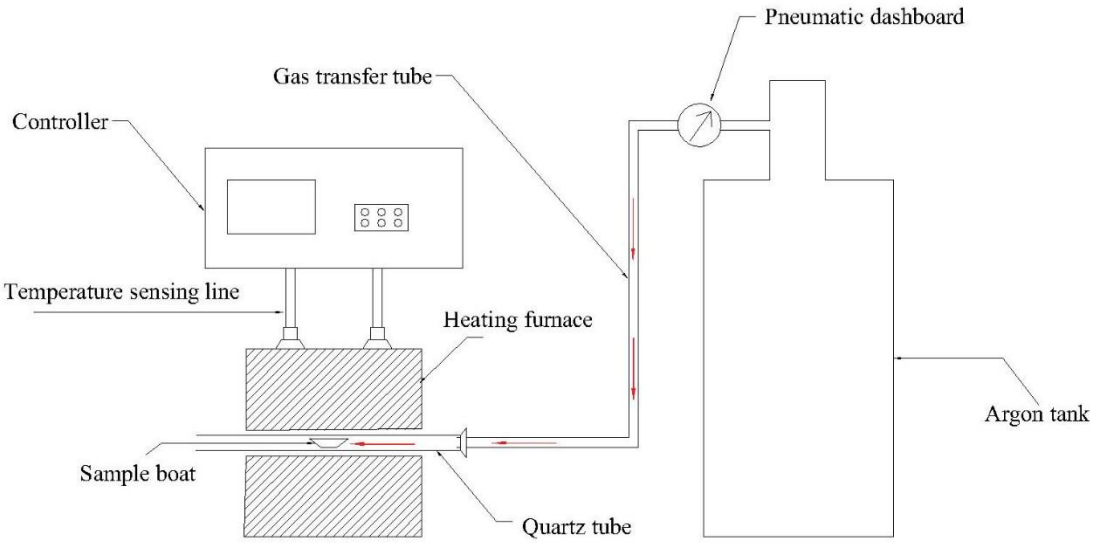


**Figure 1.** the schematic diagram of used experiment setup in the experiment

For the reduction, the pretreated WFS powders-to-magnesium powders mass ratio of 1: (0.8~1.3) was introduced into an alumina crucible and mixed uniformly. The filled crucible was placed and annealed at (400°C ~650°C) for (1~6) h with a temperature rise rate of 5°C/min in a tube furnace under Ar gas flow. The physical image of the experimental setup is shown in Fig.1. The reaction products were used only for follow-up processing without any other post-treatments.

Based on the expression of magnesiothermic reduction, the reaction products are the magnesia/Si mixture. Porous Si powders were fabricated by two-stage acid-etching. Firstly, the reaction products were stirred evenly in a 1M HCl solution for 2h at room temperature to remove MgO selectively. Then the acid-etched products were processed in an HF solution to eliminate remaining $SiO_2$. The obtained products were leached with distilled water to remove residuals for many times. Finally, the as-prepared porous Si powders were dried at 90°C in a vacuum drying oven for about 8h.

### *2.2 Characterizations*

The structural characterization of experimental materials (original WFS, the ball-milled WFS, and as-prepared porous Si powders) was performed by X-ray diffraction (XRD) analyses conducted with Bruker D8 Advance, operated at 40 kV and 40 mA with Cu Kα. The radial data (2θ) were integrated over 5~90°. The grain size and morphology characterization of materials were performed by scanning electron microscopy (SEM) equipped with energy dispersive spectroscopy (EDS), operated at 20 kV.

### *2.3 Electrochemical properties of as-prepared porous Si*

The electrochemical properties were evaluated by the test coin cells (Model CR2032). The cathode was chosen as the as-prepared porous Si, the counter electrode was chosen as metal lithium foil, the electrolyte was chosen as a 1.0 M $LiPF_6$ solution, and the separator was chosen as a polypropylene membrane. The porous Si electrode was fabricated by preparing a slurry mixed with materials at the ratio of porous Si powder: Super P: binder = 1:1:1. Such this mixture was coated onto a copper foil and then dried in a vacuum oven at 85°C. The test coin cells were assembled in a dry argon glove box. The electrochemical properties of the test coin cell were conducted with a CHI660E electrochemical workstation in a voltage range of 0.01-2.0 V (versus $Li/Li^+$) at a constant temperature.

## 3. RESULTS AND DISCUSSION

The WFS samples used in the current study were processed by the preparation route, as described details in the *Materials and Methods* section. Fig.2 explains the characterization of the morphology of WFS samples. As shown in Fig.2, the microscopic feature of the sample region using SEM revealed that, as the natural state for sand-originated, the sand grain has a clean, micro-pit of surface (Fig.2 b). The appearance of this feature shows that the WFS is necessary to treat by the leaching process of water. The impurities, such as clay or bentonite, are removed from the sand grain surface. As compared with the

new sand grain, the ball-milled sand powders have a smooth surface morphology (Fig.2 d). The grain size of powders is less than the sand-originated by the high-energy ball-milling process. Different ball-milling process conditions, such as ball-milling time and ball-milling speed, have a noticeable influence on the surface morphology and grain size of sand samples. The smaller the powders grain size is, the more favorable it is to fabricate porous Si in the final reaction. Based on these results, the WFS must be first processed to extract high-purity sand samples during the entire preparation procedure, which were then used to fabricate the final porous-Si materials.

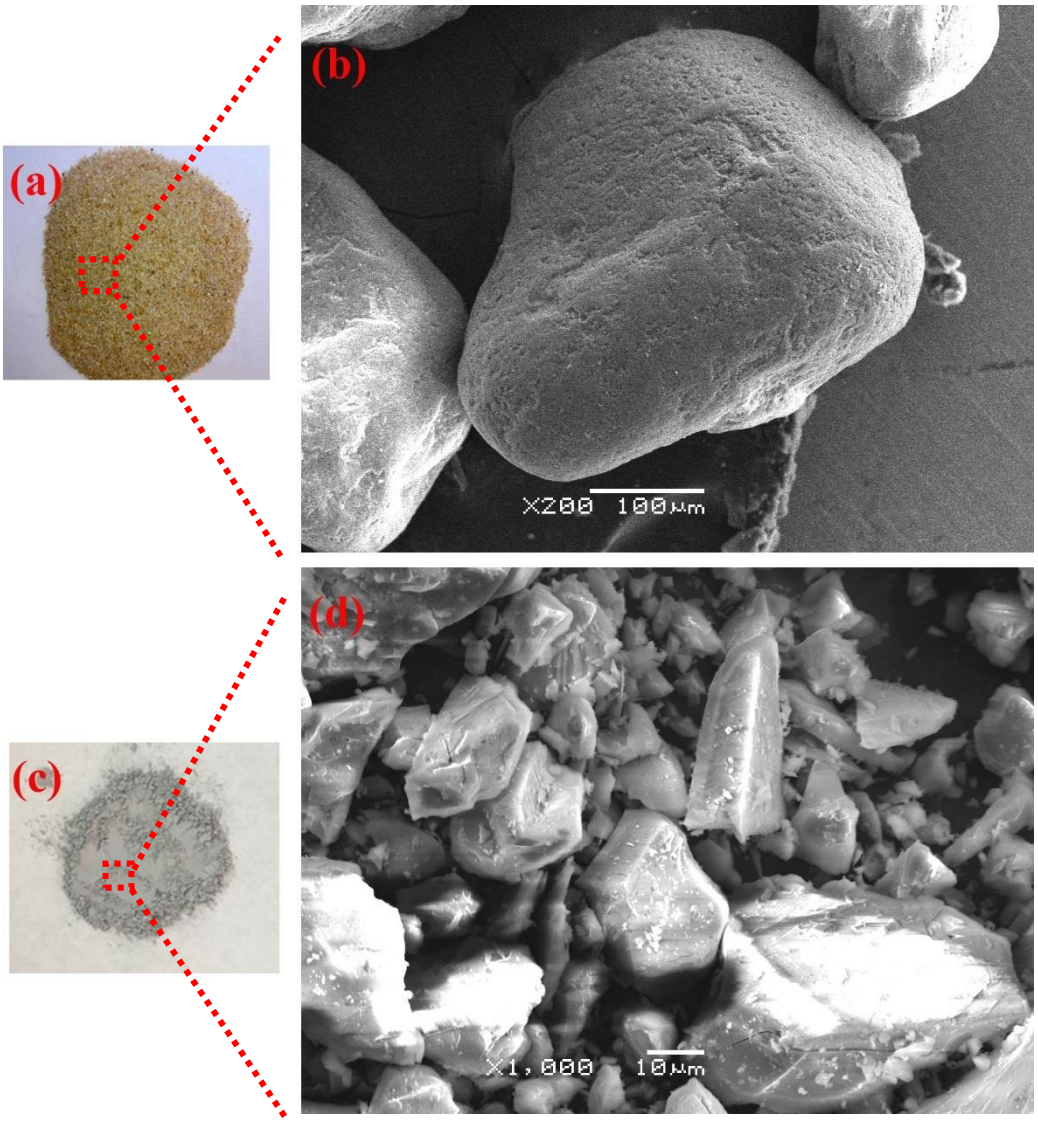


**Figure 2.** characterization of the used WFS samples: (a) images of the leached WFS; (b) sand grain morphology magnified from the box in Figure a; (c) images of the ball-milled powders sieved with a 300-mesh iron sieve; (d) powder magnified from the box in Figure c.

To verify the $SiO_2$ purity of ball-milled powders fabricated from WFS, the highly pure silica sand ($SiO_2$ >99.0%) is selected as the reference sample for the preparation of the ball-milled powders. The

detailed fabricate route is summarized details in the Materials and Methods section. Fig.3 reveals the XRD patterns of the ball-milled powders fabricated by WFS and pure silica sand, respectively. As shown in Fig.3, it is revealed that the characteristic diffraction peaks of ball-milled WFS powders are consistent with those of pure silica sand. $SiO_2$ is the primary phase, while with a small number of other impurity phases. Accordingly, the high purity of $SiO_2$ samples can be obtained by the ball milling from the foundry sand.

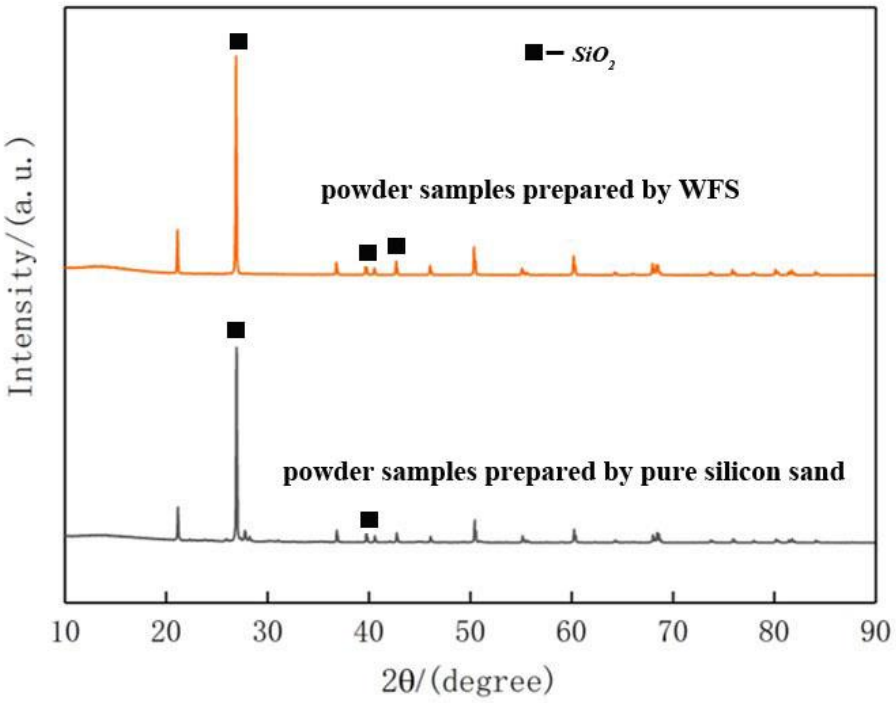


**Figure 3.** XRD patterns of the ball-milled sand powders

In the follow-up experiment, the reaction products were fabricated by the magnesiothermic reduction in a tube furnace under Ar flow a given temperature 600°C for 3h, as described details in the *Materials and Methods* section. As for the reaction in the experiment, porous silicon is fabricated by the following reaction: $2Mg(g)+SiO_2 \rightarrow 2MgO(s)+Si(s)$ . For the magnesiothermic reduction, Mg powders act as a reducing agent. The reaction products are uniformly distributed Si/MgO mixture. The effect of mass ratio (sand powders-to-Mg) is investigated for the preparation of this Si/MgO mixture. Fig.4 explains the XRD patterns of the reaction products in different mass ratios. As shown in Fig.4, there are apparent diffraction peaks of Si in the three experiments, which indicate that the designed experimental method can be considered a practical approach for the Si synthesis and preparation. The Si/MgO mixture has the primary phases (like Si and MgO) without the secondary phases (like $Mg_2Si$) in this experiment. Even more importantly, with the mass ratio increased, the diffraction peaks of MgO are apparent in the XRD pattern. As for the magnesiothermic reduction, the theoretical $SiO_2$-to-Mg mass ratio is 1:0.8. When the given mass ratio is 1:0.8, a lot of $SiO_2$ phases and a small amount of MgO phase

have appeared in the reaction products. It is revealed that an incomplete reduction has occurred due to the loss of magnesium in the experiment. When the given mass ratio is raised to 1:1.2, there is a lot of MgO phase and a small $SiO_2$ phase in the reaction products. It is indicated that excessive Mg accelerates the reduction of $SiO_2$. In other words, excessive Mg is guaranteed to complete the reduction of $SiO_2$, and especially the Mg addition amount is slightly higher than the theoretical value. Accordingly, the given mass ratio is determined as 1:1.2 in the experiment.

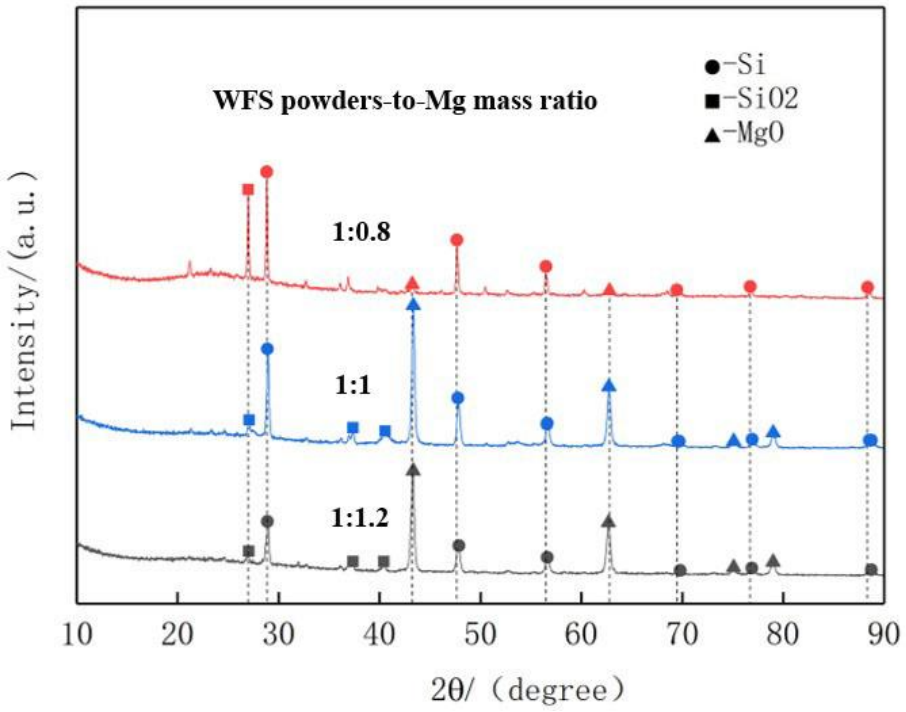


**Figure 4.** XRD patterns of the reaction products in the different mass ratio

To investigate the effect of reaction temperature for the preparation, the reaction is adopted at different given reaction temperature for 3h. The WFS powders-to-Mg mass ratio is confirmed as 1:1.2 in this experiment. Fig.5 explains the XRD patterns of the reaction products at the different reaction temperatures. As shown in Fig.5, it is indicated that the reaction temperature accelerates the reduction of $SiO_2$. When the given reaction temperature is 650°C, there are no diffraction peaks of the $SiO_2$ phase in the reaction products. Correspondingly, the diffraction peaks of the $SiO_2$ phase are visible appeared when the given reaction temperature is 550°C. In other words, the reaction products are mainly composed of Si powders if the incomplete reaction occurred. It is indicated that the higher reaction temperature accelerates the reduction of $SiO_2$. Considering the energy consumption and combining the current experiment, the given reaction temperature is determined at 650°C when the reaction time is 3h. That is perhaps more appropriate parameters of the magnesiothermic reduction.

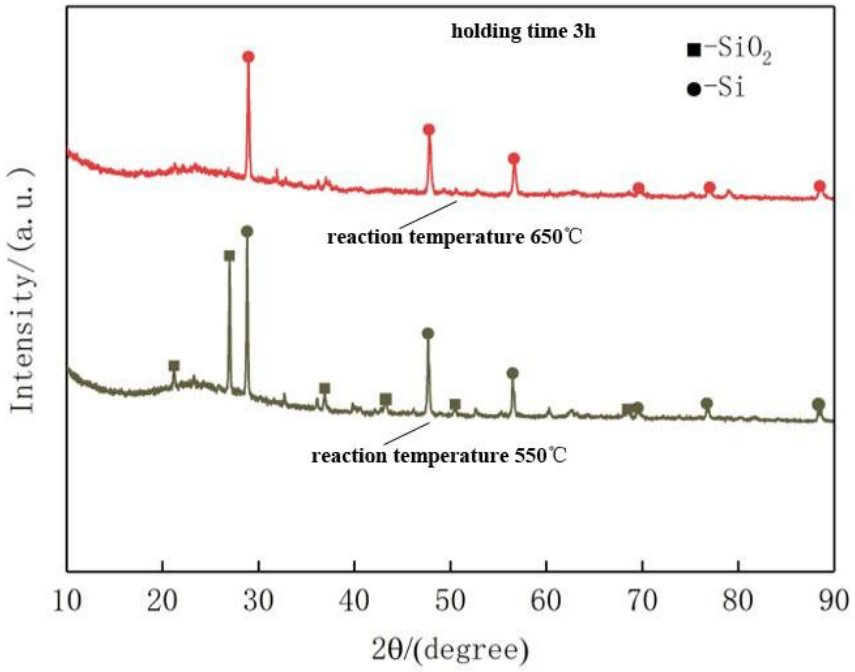


**Figure 5.** XRD patterns of the reaction products at the different reaction temperature

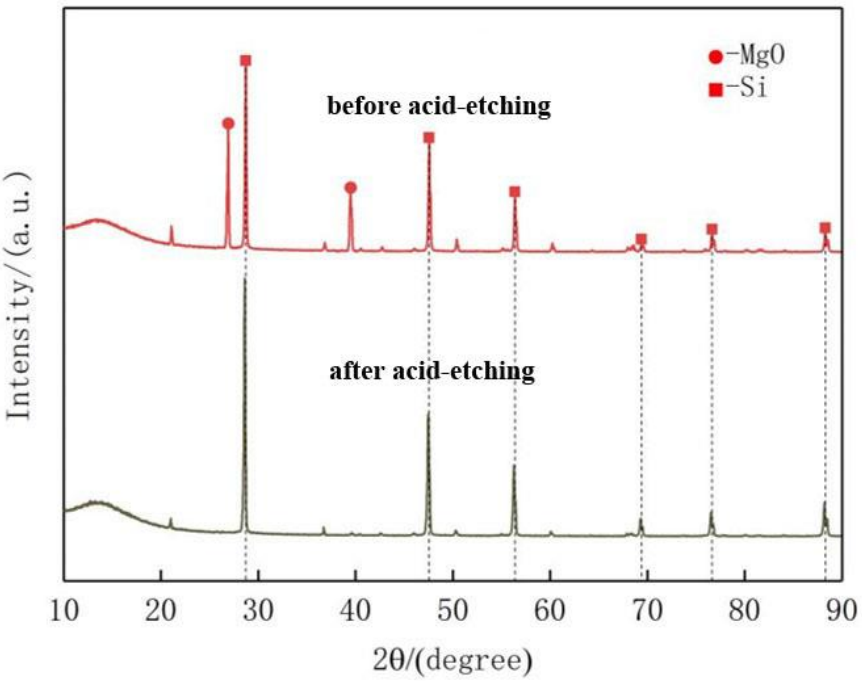


**Figure 6.** XRD patterns of the as-prepared Si powders which pretreated by acid-etching

As mentioned above, the as-prepared Si powders contain some of MgO residues. To reduce the influence of MgO for the performance of the reaction products (Si powders), the acid-etching process was adopted to remove MgO selectively. Fig.6 explains the XRD patterns of the as-prepared Si powders

pretreated by acid-etching step (before or after). As shown in Fig.6, there are some diffraction peaks of MgO before the acid-etching step for the as-prepared Si powders. Instead, after the acid-etching step, the diffraction peaks of as-prepared Si powders appear at 2θ=28°, 47°, 56°, 69°, 76° and 88°, and these diffraction peaks all correspond to the crystalline silicon diffraction peaks. The as-prepared Si powders have a good crystalline structure. Accordingly, the XRD patterns confirm the pure Si phase, as well as the MgO removal by the following chemical reaction: $MgO(s)+2HCl(aq)\rightarrow MgCl_2(aq)+H_2O$. The following acid-etching step can conclude that the WFS can be fabricated pure Si by magnesiothermic reduction. Of course, it should be noted that although a single step of magnesiothermic reduction can also fabricate Si from WFS, the acid-etching step is also necessary for the current experiment. This is mainly due to the as-prepared Si powders contain MgO residues. The acid-etching process should be utilized to remove these residues in such an experiment.

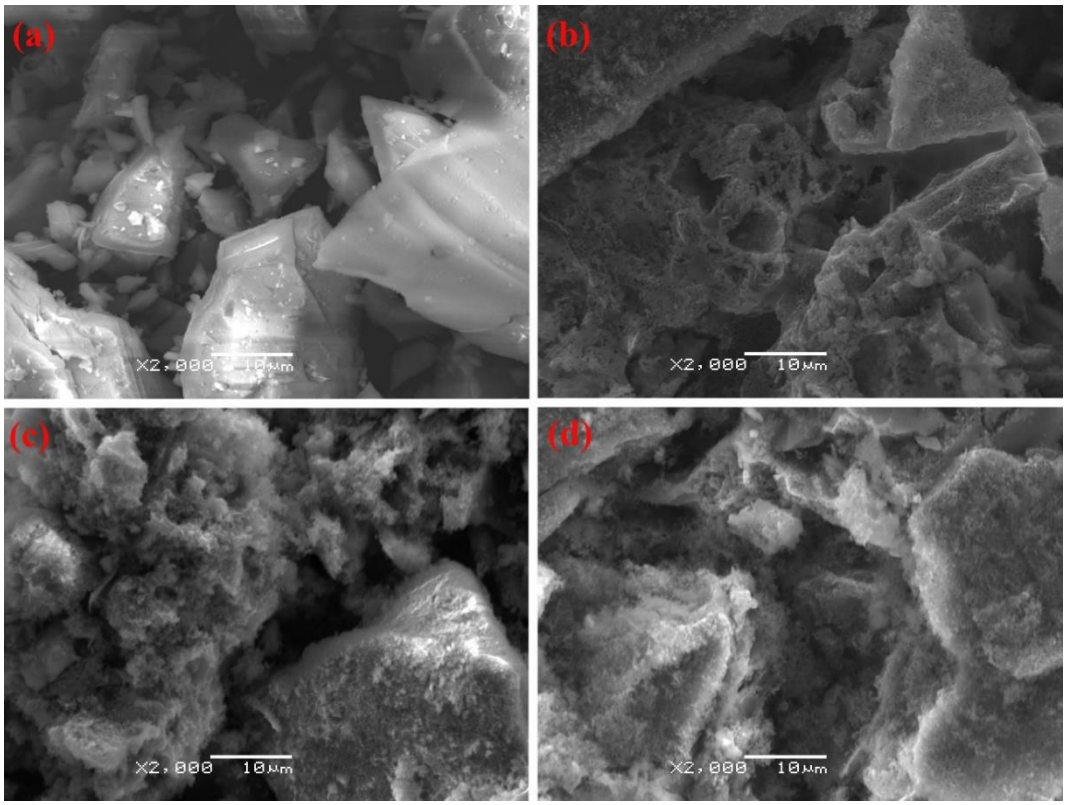


**Figure 7.** SEM images of WFS powders (a) and different regions of as-prepared Si powders(b)-(d)

The morphological features of WFS powders and as-prepared Si powders after acid-etching step was monitored using SEM measurements. Fig.7 explains the typical SEM images of WFS powders (a) and different regions of as-prepared Si powders(b)-(d), respectively. The grain surface of ball-milled WFS powders is smooth, with a sharp corner feature. The grain surface of as-prepared Si powders is unsmooth, with a porous, spongy feature. As for the as-prepared Si powders sample, it can be clearly identified for several micropores. The micropores are generated by the magnesiothermic reduction from WFS powders. This feature can be confirmed as the formation of porous Si in the experiment. The

formation mechanism of porous Si can be described as follow. At the given reaction time and temperature, the Mg in ball-milled sand powders acts as a reducing agent[41-45]. At the early stage of the reactions process, the reduction between Mg and sand powders quickly occurs at the surface of silica sand powders, due to the Mg powders are in direct contact with $SiO_2$. As the reaction progress, it is easily reduced $SiO_2$ in the surface of powders through higher temperature decomposition, but the reaction in the core region of ball-milled sand powders has become more difficult. As a result, the diffusion flux of magnesium element can be oriented from the surface to the core of ball-milled sand powders. Based on the phenomenon, magnesium elements should be continually supplied for the magnesiothermic reaction at the surface of ball-milled sand powders, resulting in the construction of a porous feature.

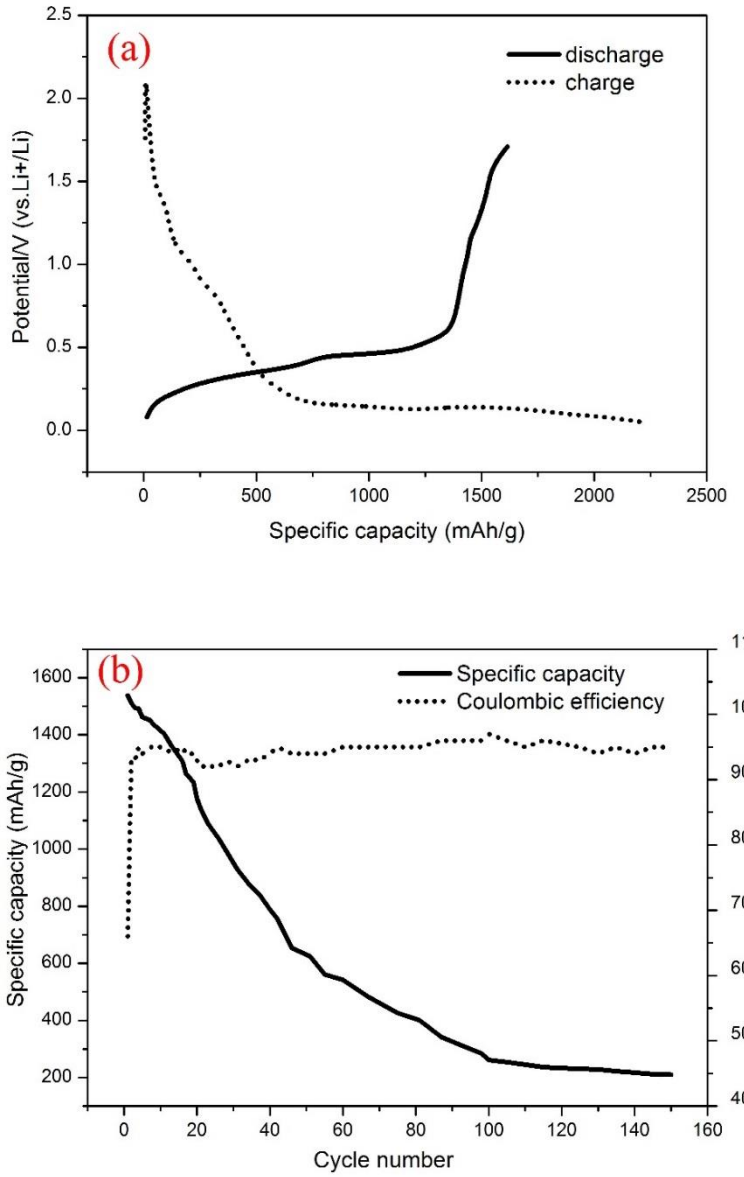


**Figure 8.** electrochemical properties of as-prepared Si electrode: (a) curves of the charge and discharge in initial one cycle, current density=100mA/g; (b) specific capacity and coulombic efficiency of an electrode as a function of cycle number

As for high-energy Li-ion batteries, the as-prepared porous Si is considered the potential for the Si-based anodes preparation. The as-prepared porous Si in this study was chosen as anodes for LIBs. Half coin cell testing was performed by adopting Li metal as the counter electrode within a voltage range of 0.01V~2.0V, and the cycling performance at a rate of 0.4 A/g was investigated. Fig.8 explains the electrochemical properties of the as-prepared porous Si electrode. As shown in Fig.8 (a), in the initial first cycle, the charge and discharge capacities are 2210 mAh/g and 1602 mAh/g, respectively. That is, the coulombic efficiency is about 72%. This is mainly due to the formation of the SEI film at the first discharge consumes some of the Li-ion, and when the $Li^+$ is embedded in the silicon, it has a considerable volume effect, which makes the Si pulverize and the Li-ion cannot be removed. There is an inclined discharge platform during the first discharge process, starting at 1.5 V, which is related to electrolyte decomposition and SEI film formation. There is an extended, flat discharge platform below 0.20 V, corresponding to partial lithiation of silicon, forming metastable amorphous $Li_xSi$. In the charging curve, the curve approaches flat between 0.3 and 0.5 v, which corresponds to the generation of amorphous Si. As shown in Fig.8(b), it is revealed that the discharge capacity of as-prepared porous Si electrodes was unstable until the number reaches 300 mAh/g after 100 cycles. The current efficiency of the charge and discharge was in the region of 92~96% in the whole process except in the first cycle. By comparing the similar Si-based anode for LIBs, the performance of as-prepared porous Si materials by the experimental method described in this study is not too bad, but there is still room for practical improvement application. As we have known, the coulombic efficiency is essential for the practical application of Li-ion battery. Based on investigating literature material, this paper makes a comparison of the as-prepared porous Si materials with similar anode materials for LIBs that were described in the literature. Table 1 compares the preparation process and the electrochemical performance of Si-based anode for Li-ion batteries. It is revealed that the initial coulombic efficiency of the Si-based anode for Li-ion battery is typically ranged from 65% to 90%.

**Table 1.** comparison of the preparation process and electrochemical performance of Si-based anode for Li-ion battery

| Materials | Preparation process | Initial first cycle capacity (mAh/g) | Initial coulombic efficiency |
|---|---|---|---|
| Micro Si powder[46] | Etching by HCl (Al-Si alloy powder) | 2378 | 66.4% |
| Nano-porous Si powders[47] | Solution processes | 1200 | 70% |
| Porous-Si/C [48] | Magnesiothermic reduction | 2500 | 75% |
| Mesoporous Si [49] | Thermal decomposition | 2660 | 72.8% |
| Carbon nanotube-Si [50] | Etching by HF | 2213 | 83.4% |
| Ferro-Si[51] | High-energy ball milling method | 1250 | 88% |
| Porous-Si (this work) | Magnesiothermic reduction (waste foundry sand) | 2210 | 72% |

## 4. CONCLUSION

To recycle waste foundry sand toward high-value applications, a novel and low-cost approach in recycling waste foundry sand for the porous Si preparation is developed in the paper. The current study demonstrates that waste foundry sand, a significant by-product in casting production, can be utilized to fabricate porous Si on a large scale. The recycling and reusing of waste foundry sand not only lead to a saving of naturally abundant sand sources but also enhance the sustainability of environmental protection. In the initial one cycle, the charge and discharge capacities are 2210 mAh/g and 1602 mAh/g, respectively. The coulombic efficiency of the as-prepared porous Si is about 72%. It is believed that this approach may have excellent potential for practical application and meet the ever-increasing demand for Si in high energy Li-ion batteries.

ACKNOWLEDGEMENTS
The authors are thankful for the financial support from the Doctoral Scientific Fund Project of Shandong Jianzhu University (No.XNBS1430).

## References

1. M.C. Staff, *Mod. Cast.*, 2018 (2018) 23-24.
2. N. Cruz, C. Briens, F. Berruti, *Resour., Conserv. Recycl.*, 54 (2009) 45-52.
3. H.M. Basar, N. Deveci Aksoy, *Constr. Build. Mater.*, 35 (2012) 508.
1. 4. R. Dańko, *Int. J. Cast Met. Res.*, 20 (2013) 228-232.
4. M. Łucarz, B. Grabowska, G. Grabowski, Arch. *Metall. Mater.*, 59 (2014) 1023.
5. C.-L. Park, B.-G. Kim, Y. Yu, *J. Hazard. Mater.*, 203-204 (2012) 176.
6. M.C. Zanetti, S. Fiore, *Resour., Conserv. Recycl.*, 38 (2002) 243-254.
7. Z. M, G. A, *Resour., Conserv. Recycl.*, 48 (2006) 16.
8. C. N, B. C, B. F, *Resour., Conserv. Recycl.*, 54 (2009) 8.
9. R. Alonso-Santurde, A. Coz, J.R. Viguri, A. Andrés, *Constr. Build. Mater.*, 27 (2012) 97.
10. R.L.P. Carnin, M.V. Folgueras, R.R. Luvizão, S.L. Correia, *Thermochim. Acta*, 543 (2012) 150.
11. G. Kaur, R. Siddique, A. Rajor, *Constr. Build. Mater.*, 29 (2012) 82.
12. Y. Xing, T. Shen, T. Guo, X. Wang, X. Xia, C. Gu, J. Tu, *J. Power Sources*, 384 (2018) 207.
13. J. Xie, L. Tong, L. Su, Y. Xu, L. Wang, Y. Wang, *J. Power Sources*, 342 (2017) 529.
14. Y. Chen, Y. Hu, Z. Shen, R. Chen, X. He, X. Zhang, *J. Power Sources*, 342 (2017) 467.
15. L.A. Berla, S.W. Lee, Y. Cui, W.D. Nix, *J. Power Sources*, 273 (2015) 41.
16. A. Casimir, H. Zhang, O. Ogoke, J.C. Amine, J. Lu, G. Wu, *Nano Energy*, 27 (2016) 359.
17. W. Lu, X. Guo, Y. Luo, Q. Li, R. Zhu, H. Pang, *Chem. Eng. J.*, 355 (2019) 208.
18. K. Baris, B. Rangeet, M. Mathieu, S. Vincent, T. Jean-Marie, C.P. Grey, *J. Am. Chem. Soc.*, 131 (2009) 9239-9249.
19. Z. Chen, L. Christensen, J.R. Dahn, *Electrochem. Commun.*, 5 (2003) 919-923.
20. H. Wu, G. Chan, J.W. Choi, I. Ryu, Y. Yao, M.T. Mcdowell, *Nat. Nanotechnol.*, 7 (2012) 310.
21. M.T. McDowell, S.W. Lee, W.D. Nix, Y. Cui, *Adv. Mater.*, 25 (2013) 4966.
22. Y. Chen, Y. Hu, Z. Shen, R. Chen, X. He, X. Zhang, Y. Zhang, K. Wu, *Electrochim. Acta*, 210 (2016) 53.
23. Z. Du, J. Li, C. Daniel, D.L. Wood, *Electrochim. Acta*, 254 (2017) 123.
24. X. Huang, X. Sui, H. Yang, R. Ren, Y. Wu, X. Guo, J. Chen, *J. Mater. Chem. A*, 6 (2018) 2593.
25. Z. Favors, W. Wang, H.H. Bay, Z. Mutlu, K. Ahmed, C. Liu, M. Ozkan, C.S.J.S.R. Ozkan, *Sci. Rep.*, 4 (2015) 5623-5623.

26. L. Shen, X. Guo, X. Fang, Z. Wang, L.J.J.o.P.S. Chen, *J. Power Sources*, 213 (2012) 229-232.
27. N. Liu, K. Huo, M.T. Mcdowell, J. Zhao, Y.J.S.R. Cui, *Sci. Rep.*, 3 (2013) 1919-1919.
28. Y. Yan, G. Lin, Z. Changbao, T. Susumu, P.A. Aken, Van, M. Joachim, *Adv. Mater.*, 22 (2010) 2247-2250.
29. A. Magasinski, P. Dixon, B. Hertzberg, A. Kvit, J. Ayala, G. Yushin, *Nat. Mater.*, 9 (2010) 353-358.
30. H.K. Liu, Z.P. Guo, J.Z. Wang, K. Konstantinov, *J. Mater. Chem.*, 20 (2010) 10055-10057.
31. B.M. Bang, H. Kim, H.K. Song, J. Cho, S. Park, *Energy Environ. Sci.*, 4 (2011) 5013-5019.
32. L. Shen, X. Guo, X. Fang, Z. Wang, L. Chen, *J. Power Sources*, 213 (2012) 229.
33. D.S. Jung, M.H. Ryou, Y.J. Sung, S.B. Park, J.W. Choi, *Proc. Natl. Acad. Sci. U. S. A.*, 110 (2013) 12229.
34. H. Wu, N. Du, X. Shi, D. Yang, *J. Power Sources*, 331 (2016) 76.
35. B. Kim, J. Ahn, Y. Oh, J. Tan, D. Lee, J.-K. Lee, J. Moon, *J. Mater. Chem. A*, 6 (2018) 3028.
36. Z. Bao, M.R. Weatherspoon, S. Shian, Y. Cai, P.D. Graham, S.M. Allan, G. Ahmad, M.B. Dickerson, B.C. Church, Z. Kang, H.W. Abernathy Iii, C.J. Summers, M. Liu, K.H. Sandhage, *Nat.*, 446 (2007) 172.
37. J. Erlebacher, M.J. Aziz, A. Karma, N. Dimitrov, K. Sieradzki, *Nat.*, 410 (2011) 450.
38. M. Kunduraci, *J Solid State Electrochem*, 20 (2016) 2105.
39. W. McSweeney, H. Geaney, C. O'Dwyer, *Nano Res.*, 8 (2015) 1395-1442.
40. J. Liang, X. Li, Z. Hou, C. Guo, Y. Zhu, Y. Qian, *Chem. Commun.*, 51 (2015) 7230-7233.
41. J. Ahn, D.-H. Lee, M.S. Kang, K.-J. Lee, J.-K. Lee, Y.-E. Sung, W.C. Yoo, *Electrochim. Acta*, 245 (2017) 893-901.
42. N. Lin, L. Wang, J. Zhou, J. Zhou, Y. Han, Y. Zhu, Y. Qian, C. Cao, *J. Mater. Chem. A*, 3 (2015) 11199-11202.
43. L. Wang, N. Lin, J. Zhou, Y. Zhu, Y. Qian, *Chem. Commun.*, 51 (2015) 2345-2348.
44. Z. Hou, X. Zhang, J. Liang, X. Lia, X. Yan, Y. Zhu, Y. Qian, *RSC Adv.*, 5 (2015) 71355-71359.
45. Z. Jiang, C. Li, S. Hao, K. Zhu, P. Zhang, *Electrochim. Acta*, 115 (2014) 393-397.
46. H. Wu, G. Yu, L. Pan, N. Liu, M.T. Mcdowell, Z. Bao, Y. Cui, *Nat. Commun.*, 4 (2013) 1943.
47. H. Jia, J. Zheng, J. Song, L. Luo, R. Yi, L. Estevez, W. Zhao, R.L. Patel, X. Li, J. Zhang, *Nano Energy*, 50 (2018) 589-597.
48. L. Sun, F. Wang, T. Su, H. Du, *ACS Appl. Mater. Interfaces*, 9 (2017) 40386-40393.
49. M.J. Choi, Y. Xiao, J.Y. Hwang, I. Belharouak, Y. Sun, *J. Power Sources*, 348 (2017) 302-310.
50. H. Li, F. Cheng, Z. Zhu, H. Bai, Z. Tao, J. Chen, *J. Alloys Compd.*, 509 (2011) 2919-2923.